Mesenchymal Stem Cell–Derived Small Extracellular Vesicles Promote Neuroprotection in Rodent Models of Glaucoma

Ben Mead,[1] Juan Amaral,[2] and Stanislav Tomarev[1]

[1]Section of Retinal Ganglion Cell Biology, Laboratory of Retinal Cell and Molecular Biology, National Eye Institute, National Institutes of Health, Bethesda, Maryland, United States
[2]Unit on Ocular Stem Cell & Translational Research, National Eye Institute, National Institutes of Health, Bethesda, Maryland, United States

Correspondence: Ben Mead, Section of Retinal Ganglion Cell Biology, Laboratory of Retinal Cell and Molecular Biology, National Eye Institute, National Institutes of Health, Bethesda, Maryland, 20892, USA; ben.mead@nih.gov.
Stanislav Tomarev, Section of Retinal Ganglion Cell Biology, Laboratory of Retinal Cell and Molecular Biology, National Eye Institute, National Institutes of Health, Bethesda, Maryland, 20892, USA; TomarevS@nei.nih.gov.

Submitted: August 23, 2017
Accepted: January 4, 2018

Citation: Mead B, Amaral J, Tomarev S. Mesenchymal stem cell–derived small extracellular vesicles promote neuroprotection in rodent models of glaucoma. *Invest Ophthalmol Vis Sci*. 2018;59:702–714. https://doi.org/10.1167/iovs.17-22855

Purpose. To investigate the benefit of bone marrow mesenchymal stem cell (BMSC)-derived small extracellular vesicles (sEV) as an intravitreal (ivit) therapy in two rat models of glaucoma and to determine and identify candidate miRNA involved in the mechanism.

Methods. sEV were isolated from human BMSC and fibroblasts and ivit injected into adult rats after induction of elevated IOP. IOP was elevated using either intracameral injection of microbeads or laser photocoagulation of circumferential limbal vessels and the trabecular meshwork. Retinal nerve fiber layer (RNFL) thickness was measured using optical coherence tomography, positive scotopic threshold response (pSTR) recorded using ERG, and RNA binding protein with multiple splicing ($RBPMS^+$) retinal ganglion cell (RGC) counted using retinal wholemounts. sEV miRNA were sequenced using RNAseq.

Results. sEV isolated from BMSC promoted significant neuroprotection of RGC while preventing RNFL degenerative thinning and loss of pSTR. sEV proved therapeutically efficacious when ivit injected every week or every month, but ineffective with longer delays between treatments. Knockdown of Argonaute2 (AGO2), a protein critical for miRNA function and packing into sEV prior to sEV isolation, significantly attenuated the above effects. Addition of BMSC sEV (but not fibroblast sEV) reduced death of cultured purified RGC. RNAseq identified 43 miRNA upregulated in BMSC sEV in comparison to fibroblast sEV, which yielded no neuroprotective effects.

Conclusions. Injection of BMSC-derived sEV into the vitreous provided significant therapeutic benefit to glaucomatous eyes. The neuroprotective effect of sEV, at least partially, may be explained by direct action on RGC through miRNA-dependent mechanisms.

Keywords: glaucoma, mesenchymal stem cells, extracellular vesicles, exosomes, retinal ganglion cells, miRNA

Glaucoma is one of the world's leading causes of irreversible blindness and is characterized by the slow progressive degeneration of retinal ganglion cells (RGC) and their axons.[1] RGC operate as the final stage in the phototransductive visual pathway of the retina, tasked with the projection of electrochemical information to the brain along their axons, which make up the optic nerve. RGC are irreplaceable, making their dysfunction and subsequent loss a severe detriment to vision and thus, quality of life. While current therapies can successfully reduce IOP, the critical risk factor associated with glaucoma, no neuroprotective strategies currently exist.

Mesenchymal stem cells (MSC) are a multipotent stromal cell residing in mesenchymal tissues such as bone marrow (BMSC),[2] adipose (ADSC),[3] umbilical blood (UCB-MSC),[4] and dental pulp.[5] Their neuroprotective efficacy in retinal injury models has been demonstrated by us[6–9] as well as independent research groups,[10–12] and are currently undergoing clinical trials for retinal degenerative diseases such as glaucoma.[13] The mechanism of action is exclusively paracrine, through the secretion of neuroprotective factors as opposed to RGC replacement. MSC secrete a large abundance of factors, of which several neuroprotective candidates have been identified including brain-derived neurotrophic factor (BDNF) and platelet-derived growth factor (PDGF).[7,14]

Extracellular vesicles (EV) include exosomes, microvesicles, and apoptotic bodies and were described decades ago as being secreted from most cell types both by outward budding of the plasma membrane as well as intracellular formation within multivesicular endosomes before secretion into the extracellular space.[15] The formation of the vesicle as well as the loading of cargo is reliant on a complex of 30 proteins referred to as Endosomal Sorting Complex Required for Transport (ESCRT). Exosomes contain mRNA, miRNA, lipids, and protein and can be easily isolated from various bodily fluids as well as conditioned medium in vitro.[15,16] Exosomes are typically defined by their size of less than 150 nm although a 220 nm threshold is often used as the sample is passed through 220-nm porous filter.[17] As this preparation includes nonexosomal EV, this population will be referred to as small EVs (sEV) from this point. Originally thought to be a mechanism solely for the

removal of waste, sEV have now been demonstrated to deliver their cargo to nearby cells that translate the mRNA into proteins, as well as have gene expression downregulated by the sEV-derived miRNA.[18] Therefore, irrespective of the receptors a recipient cell expresses, gene expression can be regulated by sEV-mediated cell-to-cell communication.

miRNA are small RNA molecules that are processed and incorporated into the RNA-induced silencing complex (RISC) composed of Dicer, TRBP, and Argonaute2 (AGO2), its catalytic center.[19] Binding of the miRNA to the 3′ untranslated region of mRNA leads to repression of translation and a single miRNA can repress the translation of several hundred mRNA. AGO2 is integral to miRNA function as well as to the packaging of miRNA into sEV.[20] Interestingly, the function of exosomal miRNA is dependent on AGO2 derived from the origin cell/sEV, AGO2 in the recipient cell is not involved in the exosomal-derived miRNA function. Therefore, knockdown of AGO2 in host cells allows the isolation and testing of miRNA-depleted sEV.[21,22]

The secretome of BMSC is responsible for their therapeutic efficacy and exosomes/sEV, considered part of the secretome, have been proposed to orchestrate some of these effects.[23–25] Interestingly, MSC sEV are enriched for select miRNA relative to MSC, suggesting the loading and packaging of RNA into sEV is an active and specific process.[26] Several studies have begun to test MSC sEV in a variety of disease models including ocular pathologies. Intravenous BMSC sEV treatment in a mouse model of experimental autoimmune uveitis prevented significant retinal structural damage, inflammatory cell infiltration, and proinflammatory cytokine elevation.[27] BMSC-derived sEV were found to be just as effective as BMSC, suggesting they are the active component mediating the therapeutic effect. Similarly, periocular injections of MSC sEV in rats with experimental autoimmune uveitis reduced the infiltration of T cell subsets and other inflammatory cells in the eyes.[28]

In a mouse model of diabetic nephropathy, systemic administration of BMSC, BMSC-conditioned medium, or BMSC-derived sEV elicited a therapeutic effect and promoted survival of tubular epithelial cells.[29] Intravitreal (ivit) injections of MSC-derived sEV in mice ameliorated retina laser injury partially by inhibition of monocyte chemotactic protein.[30]

In many cases, the therapeutic effects elicited by BMSC sEV have been attributed to their miRNA cargo. In a mouse model of myocardial infarction, intravenous,[31] or subcutaneous[32] delivery of MSC sEV improved angiogenesis and subsequent cardiac function. This effect was mediated through miRNA and in particular, miRNA-210 and its interaction with the gene *Efna3*.[32] An in vitro study demonstrated that UCB-MSC– and BMSC-derived sEV protect kidney tubular epithelial cells through the action of miRNA including *MIR-23A*, *MIR-126*, and *MIR-296*.[33] In line with these observations, our previous study showed that BMSC sEV demonstrate a significant neuroprotective effect on injured RGC after optic nerve crush (ONC), an effect that was abrogated following the depletion of miRNA from sEV.[22]

The present study aimed to test BMSC sEV in a more clinically relevant setting by using two rat models of glaucoma, and aimed to determine candidate miRNA responsible for this effect.

Methods

Animals

Adult female outbred Sprague-Dawley rats weighing 150 to 200 g (Charles River, Wilmington, MA, USA) were maintained in accordance with guidelines described in the ARVO Statement for the Use of Animals in Ophthalmic and Vision Research, using protocols approved by the National Eye Institute Committee on the Use and Care of Animals.

Animals were kept at 21°C and 55% humidity under a 12-hours light and dark cycle, given food/water ad libitum and were under constant supervision from trained staff. Animals were euthanized by rising concentrations of CO_2 before extraction of retinae.

Materials

All reagents were purchased from Sigma (Allentown, PA, USA) unless otherwise specified.

BMSC Cultures

Human $CD29^+/CD44^+/CD73^+/CD90^+/CD45^-$ BMSC (confirmed by supplier; Lonza, Walkersville, MD, USA) from three donors were pooled and cultured in Dulbecco's modified Eagle's medium (DMEM) containing 1% penicillin/streptomycin and 10% exosome-depleted fetal bovine serum (Thermo Fisher Scientific, Cincinnati, OH, USA). Cell cultures were maintained at 37°C in 5% CO_2 with medium changed every 3 days and cells passaged with 0.05% trypsin/EDTA when 80% confluent. Human dermal fibroblasts (Lonza) were grown in the above conditions and used as a control. For all experiments, BMSC and dermal fibroblasts were used at passage two through five.

Transfection and Confirmation of Knockdown

For a subgroup of animals, BMSC were transfected using Lipofectamine 3000 (Thermo Fisher) per the manufacturer's protocol. Briefly, 70% confluent BMSC grown in Opti-MEM medium were incubated with Lipofectamine 3000 reagent and either siRNA against *AGO2* (SiAgo2, #4392420/assay id s25931; Thermo Fisher Scientific) or a scrambled control siRNA (#4390843; SiScr) for 48 hours. AGO2 knockdown (>70%) was confirmed by Western blotting like previously described[22] (Supplementary Fig. S1).

Exosome/sEV Isolation and Quantification

Exosomes were isolated from BMSC and fibroblasts using ExoQuick-TC (System Biosciences, Mountain View, CA, USA) per the manufacturer's instructions. Briefly, conditioned medium was centrifuged at 3000*g* for 15 minutes to remove cells and debris, incubated with ExoQuick reagent overnight at 4°C (1:10 ratio with medium), centrifuged at 1500*g* for 15 minutes a final time before the exosome pellet is resuspended in sterile PBS. The exosome preparation is passed through a 0.22-μm filter to remove any large extracellular vesicles (microvesicles and apoptotic bodies). Because it is expected some nonexosomal vesicles remain in the preparation, we refer to the exosomes used in this study as sEV. Using Western blot, exosomes were characterized by their positive staining for the exosome/sEV markers Syntenin-1 and CD63 and negative staining for high-/low-density lipoprotein markers ApoA1 and ApoB (Supplementary Fig. S2). Briefly, sEV were lysed in passive lysis buffer (#E1531; Promega, Madison, WI, USA) before protein concentration was determined by BCA protein assay (Thermo Fisher). Protein samples (20 μg) were separated on 4% to 12% Bis-Tris protein gels at 150 V for 40 minutes. Proteins were transferred to polyvinylidene fluoride membranes, blocked in 10% Western blot blocking buffer (Roche, Basel, Switzerland) in Tris-buffered saline (TBS), stained overnight in primary antibody (Table 1) diluted in TBS, washed 3 × 5 minutes in TBST, stained for 1 hour with secondary

Investigative Ophthalmology & Visual Science

Table 1. Antibodies Used in Immunohistochemistry (IHC), Immunocytochemistry (ICC), and Western Blot (WB)

Antigen	Dilution	Supplier	Catalogue No.
RBPMS	1:500 (IHC)	Thermo Fisher	#ABN-1376
βIII-tubulin	1:500 (ICC)	Sigma	#T-8660
AGO2	1:1000 (WB)	Thermo Fisher	#MA5-14861
Syntentin-1	1:1000 (WB)	Abcam (Cambridge, MA, USA)	#Ab133267
CD63	1:1000 (WB)	System Biosciences	#Exoab-CD63-A1
ApoA1	1:1000 (WB)	Abcam	#ab7613
ApoB	1:1000 (WB)	Abcam	#ab20737
HSC70	1:5000 (WB)	Santa Cruz (Dallas, TX, USA)	#sc-7298
Mouse IgG HRP	1:2000 (WB)	GE Healthcare (Waldorf, MD, USA)	#NA-931
Guinea Pig IgG 546	1:400 (IHC)	Thermo Fisher	#A-11074
Mouse IgG 488	1:400 (ICC)	Thermo Fisher	#A-11001
Mouse IgG HRP	1:2000 (WB)	GE Healthcare	#NA-931
Rabbit IgG HRP	1:10,000 (WB)	Cell Signaling (Danvers, MA, USA)	#7074

antibody (Table 1) in TBS, washed 3 × 5 minutes in TBST before detection with Immobilon ECL reagents (Millipore, Burlington, MA, USA). Densitometry of Western blot bands were analysed using ImageJ software (http://imagej.nih.gov/ij/; provided in the public domain by the National Institutes of Health, Bethesda, MD, USA). sEV were derived from BMSC pooled from 3 donors and this pooled sample of sEV was assayed in triplicate by Western blot and used throughout the remainder of the study.

The concentration and size distribution of sEV were characterized using a NanoSight LM10 instrument (Malvern, Worcester, MA, USA), equipped with a 405 nm LM12 module and EM-CCD camera (DL-658-OEM-630; Andor, Concord, MA, USA). Three videos were captured per sample with a camera level of 10. Videos were analyzed with a detection threshold of two, automatic blur size and 12.9- to 13.1-pix maximum jump size. Slider gain was set to 80 and a total of 567 frames were taken.

Isolation, Purification, and Culture of Retinal Ganglion Cells

Eight well chamber slides (Thermo Fisher Scientific) were precoated with 100 μg/mL poly-D-lysine for 60 minutes and then with 20 μg/mL laminin for 30 minutes. After culling and ocular dissection, the retinae of female Sprague-Dawley were minced in 1.25 mL of papain (20 U/mL; as per manufacturer's instructions, #LK003150; Worthington Biochem, Lakewood, NJ, USA) containing 50 μg/mL of DNase I (62.5 μL; Worthington Biochem) and incubated for 90 minutes at 37°C. The retinal cell suspension was centrifuged at 300*g* for 5 minutes and the pellet resuspended in 1.575 mL of Earle's balanced salt solution (Worthington Biochem) containing 1.1 mg/mL of reconstituted albumin ovomucoid inhibitor (150 μL; Worthington Biochem) and 56 μg/mL of DNase I (75 μL). After adding to the top of 2.5 mL of albumin ovomucoid inhibitor (10 mg/mL) to form a discontinuous density gradient, the retinal cell suspension was centrifuged at 70*g* for 6 minutes and the cell pellet resuspended in 1 mL of PBS.

RGC were purified from the retinal suspension using CD90.1 magnetic beads as per the manufacturer's instructions (#130-096-209; Miltenyi Biotec, Auburn, CA, USA). Briefly, retinal cells are incubated with CD90.1 enrichment and CD11b depletion antibodies conjugated to magnetic beads. Following depletion, the retinal suspension is passed through a magnetized column and the enriched RGC are collected and plated at a density 5000 RGC/well in supplemented Neurobasal-A (25 mL Neurobasal-A [Thermo Fisher Scientific], 1X concentration of B27 supplement [Life Technologies, Carlsbad, CA, USA], 0.5 mM of L-glutamine [62.5 μL; Thermo Fisher Scientific], and 50 μg/mL of gentamycin [125 μL; Thermo Fisher Scientific]). We confirmed a >99% RGC purity by immunocytochemistry, staining for RBPMS (data not shown).

In Vivo Experimental Design

The experimental design is shown schematically in Figure 1A. Seventy rats were divided into three groups: Group 1 consisted of five uninjured/untreated animals; Group 2 consisted of 30 rats with ocular hypertension induced by intracameral (ic) injection of microbeads; Group 3 consisted of 35 rats with ocular hypertension induced by laser photocoagulation of the trabecular meshwork (TM) and limbal vessels. Induction of the model as well as treatment with ivit sEV (BMSC or fibroblasts) were performed bilaterally and began on day 0 with some animals further receiving a weekly treatment. While it is not possible to treat Group 3 monthly, as the experimental length is 21 days, Group 2, which is a 56-day experiment also received monthly injections. Along with BMSC and fibroblast sEV treatments, Group 3 also received sEV derived from MSC transfected with SiAgo2 or SiScr. To make up for any animals/tissue that were unusable at the end of the study (due to animal deaths, surgical problems, lack of ocular hypertension, or wholemounting errors), additional animals were run to ensure each treatment subgroup was made up of five animals/10 eyes.

Induction of Ocular Hypertension With Intracameral Microbeads

Ocular hypertension was induced in Group 2 by ic injection of microbeads as previously described.[34] Anesthesia was induced with 5% Isoflurane (Baxter Healthcare Corp, Deerfield, IL, USA)/1.5 L per minute O_2 and maintained at 3.5% throughout the procedure. Using a 15° blade (Fine Science Tools, Reading, PA, USA) a small 2-mm incision was made at the peripheral cornea and aqueous humour was allowed to exude. Using the same incision site, a 10-μL solution of microbeads was administered with a glass micropipette, produced in-house from a glass capillary rod (Harvard Apparatus, Kent, UK) using a Flaming-Brown micropipette puller (Sutter Instruments, Novato, CA, USA). The microbead solution was loaded into the microneedle immediately before injection and consisted of 5 μL of 6-μm beads (polybead polystyrene, Cat#07312; Polysciences, Inc., Warrington, PA, USA) followed by 5 μL of 10-μm beads (polybead polystyrene, Cat#17136; Polysciences, Inc.), both at concentrations of 2×10^8/mL. Administration was made slowly and the needle was retracted with a 2-minute delay to minimize leakage. Due to the variable translucency of

A

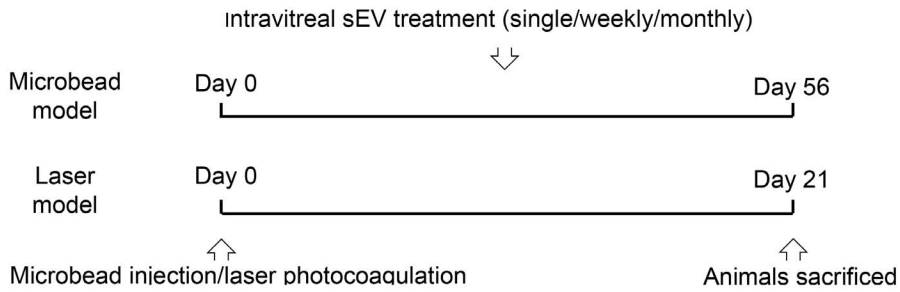

Group	No. of animals (eyes)	Injury	Treatment
1	5 (10)	Uninjured	Untreated
2	5 (10)	Microbeads	Untreated
2	5 (10)	Microbeads	Single (day 0) BMSC-derived sEV
2	5 (10)	Microbeads	Monthly BMSC-derived sEV
2	5 (10)	Microbeads	Weekly BMSC-derived sEV
2	5 (10)	Microbeads	Monthly fibroblast-derived sEV
2	5 (10)	Microbeads	Weekly fibroblast-derived sEV
3	5 (10)	Laser	Untreated
3	5 (10)	Laser	Single (day 0) BMSC-derived sEV
3	5 (10)	Laser	Weekly BMSC-derived sEV
3	5 (10)	Laser	Weekly siAgo2 BMSC-derived sEV
3	5 (10)	Laser	Weekly siScr BMSC-derived sEV
3	5 (10)	Laser	Single (day 0) fibroblast-derived sEV
3	5 (10)	Laser	Weekly fibroblast-derived sEV

B

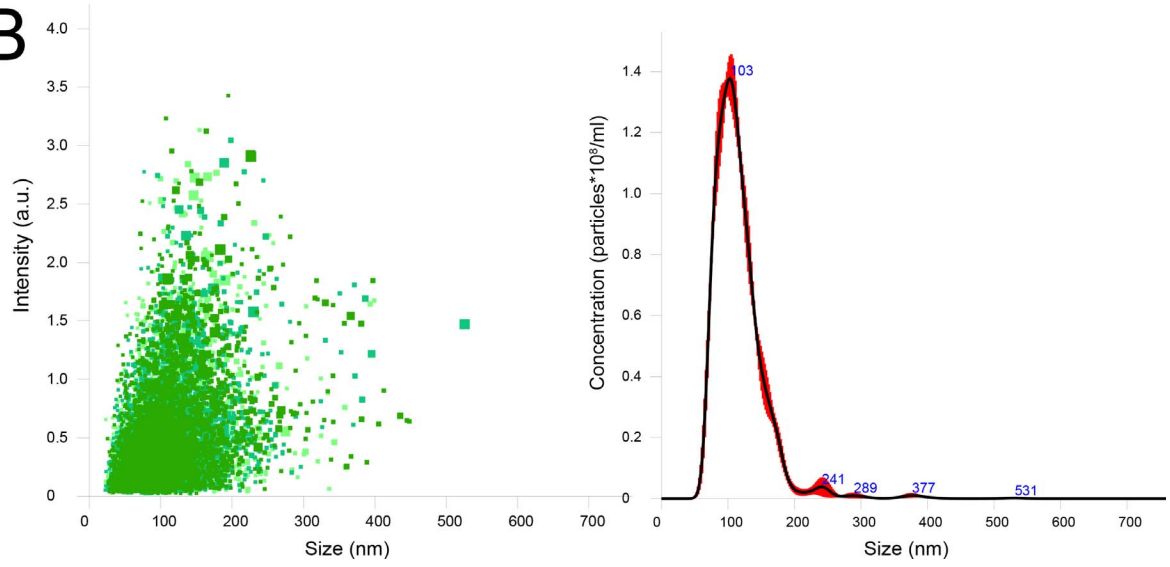

Figure 1. Experimental design of study and exosome isolation. **(A)** Timeline and groupings of study, detailing the number of animals (eyes) per group, the two glaucoma models used and the sEV treatment schedule. **(B)** Nanosight analysis of extracellular vesicles isolated from BMSC, demonstrating their size and relative quantity.

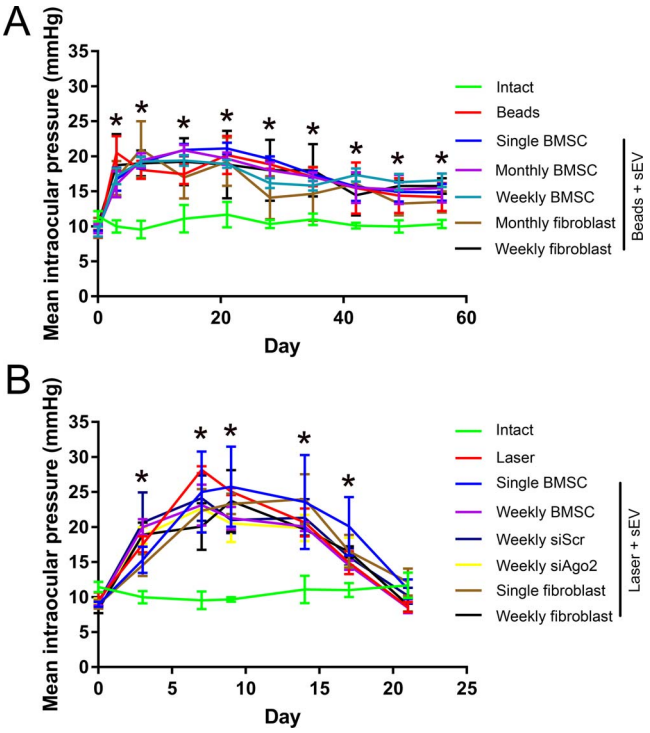

FIGURE 2. IOP measurements in the two glaucoma models. (**A**) Mean ± SEM IOP (mm Hg) of healthy animals (*green*) and animals receiving ic injection of microbeads and ivit sEV treatments. (**B**) Mean IOP of healthy animals (*green*) and animals receiving laser photocoagulation of the trabecular meshwork/limbal vessels and ivit sEV treatments. *Asterisks* represent significant difference between intact/control and experimental groups ($P < 0.05$).

the eye after microbead injection, reliable ERG and optical coherence tomography (OCT) measurements were not possible.

Induction of Ocular Hypertension With Laser Photocoagulation

Ocular hypertension was induced in Group 3 by laser photocoagulation of the TM and circumferential limbal vessels as previously described.[35] Anesthesia was induced with intraperitoneal injection of ketamine (100 mg/kg; Putney, Inc., Portland, ME, USA)/xylazine (10 mg/kg; Lloyd, Inc., Shenandoah, IA, USA). Pupil constriction and subsequent opening of the iridocorneal angle was achieved with 4% pilocarpine hydrochloride ophthalmic solution (Sandoz, Princeton, NJ, USA). An OcuLight GLx 532-nm laser (Iridex, Mountain View, CA, USA) was used to deliver laser burns at 0.3 W, at a spot size of 100 μm, and duration of 0.5 seconds. Three locations were photocoagulated: approximately 270° of the circumferential limbal vessels, episcleral veins branching from these limbal vessels, and finally, a transscleral/transcorneal 360° burn of the TM/iridocorneal angle. Nasal vasculature was left uninjured to prevent ischemia.

Intraocular Pressure Recording

IOP were recorded for all rats using a Tonolab rebound tonometer (Colonial Medical Supply, Franconia, NH, USA). IOP was recorded under isoflurane-induced anesthesia during the same 3- hour window each day, sampled 18 times and averaged for each individual recording.

Intravitreal Delivery of sEV

Under isoflurane-induced anesthesia, sEV were injected into the vitreous, just posterior to the limbus using glass micropipette. A 5-μL volume of sterile phosphate-buffered saline (sPBS) loaded with 3×10^9 sEV was injected slowly and the needle was retracted after a 1-minute delay to minimize backflow. The concentration was chosen based on our previous study[22] that demonstrated efficacy.

Electroretinography Measurements of the Positive Scotopic Threshold Response

ERG was recorded using the Espion Ganzfeld full-field system (Diagnosys LLC, Lowell, MA, USA) on day 0 before induction of ocular hypertension, and on day 56/21 (Groups 2 and 3, respectively) before animals were killed. Rats were dark adapted for 12 hours overnight and prepared for ERG recording under dim red light (>630 nm). Anesthesia was induced with intraperitoneal injection of ketamine/xylazine and eyes dilated with tropicamide. Scotopic flash ERG was recorded from −5.5 to +10 log units with respect to standard flash in half log-unit steps. ERG traces were analyzed using in built Espion software and the amplitude (with respect to baseline) was used as a measure of rat visual function. Traces at a light intensity of 1×10^{-5} mcd/s were chosen for analysis as they gave a clean, unambiguous pSTR 100 ms after stimulus. An individual masked to the treatment groups performed all readings and analysis.

Optical Coherence Tomography Measurements of the Retinal Nerve Fiber Layer

OCT was performed on rats under anesthesia (intraperitoneal ketamine/xylazine) on day 0 before induction of ocular hypertension, and on day 56/21 (Groups 2 and 3, respectively) before animals were killed. A Spectralis HRA3 confocal scanning laser ophthalmoscope (Heidelberg Engineering, Heidelberg, Germany) was used to take images of the retina around the optic nerve head and in-built software segmented the retinal nerve fiber layer (RNFL) and quantified the thickness. Segmentation was manually adjusted (by an individual masked to the treatments groups) when necessary to prevent inclusion of blood vessels that populate the RNFL.

RGC Counts in Retinal Wholemounts

Rats were euthanized at 56/21 days (Groups 2 and 3, respectively) by rising concentration of CO_2, and perfused intracardially with 4% paraformaldehyde (PFA) in PBS. Eyes were enucleated and retinae dissected and immersion post-fixed in 4% PFA for 1 hour at 4°C. Wholemounted retinae were permeabilized in 0.5% Triton X-100 in PBS for 15 minutes at −70°C, washed in fresh Triton X-100 for a further 15 minutes before incubation with primary antibody diluted in whole-mount antibody diluting buffer (wADB2% bovine serum albumin, 2% Triton X-100 in PBS) overnight at 4°C and, the following day, were washed 3 × 10 minutes in PBS and incubated with secondary antibodies in wADB for 2 hours at room temperature. After 2 hours, retinae were washed for 3 × 10 minutes in PBS and mounted vitreous side up on superfrost glass slides (Superfrost Plus; Fisher Scientific, Pittsburgh, PA, USA), facilitated by four equidistant cuts into the peripheral retina. Slides were allowed to air dry before mounting in Vectorshield medium (Vector Laboratories, Peterborough, UK) and applying cover slips. The antibodies used are detailed in Table 1.

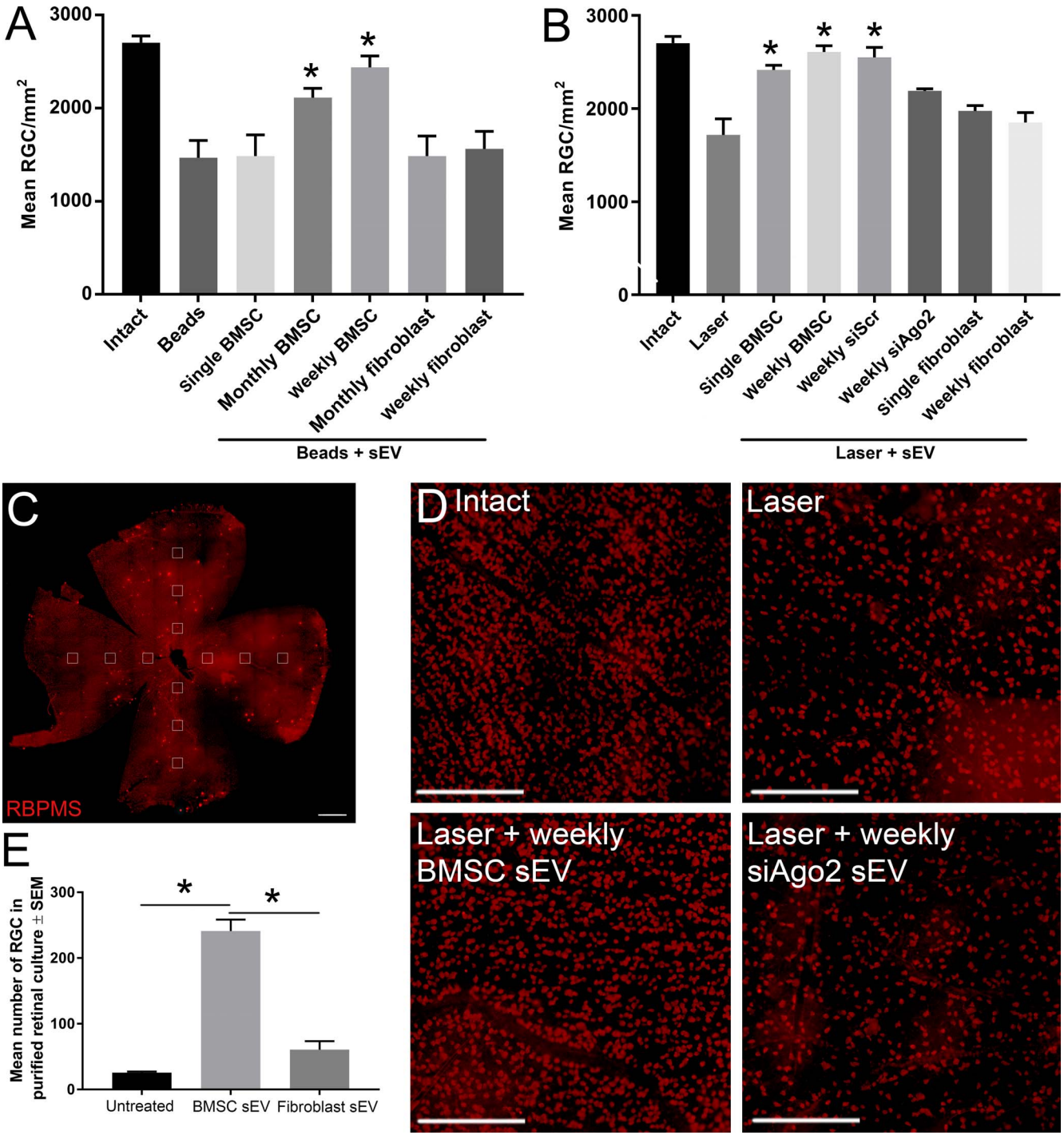

Figure 3. Surviving RBPMS$^+$ RGC count. (**A**, **B**) Mean ± SEM number of surviving RBPMS$^+$ RGC 56 days after ic microbead injection (**A**) or 21 days after laser photocoagulation (**B**). Counts were conducted in a 0.33-mm^2 region of retinal wholemounts, calculated as a composite average of 12 images taken at 1-, 2-, and 3-mm distances from the optic nerve head, four images per retinal petal (**C**; *scale bar*, 1 mm). *Asterisks* indicate significant difference from injured/untreated at $P < 0.05$. (**D**) Representative images of RBPMS$^+$ RGC from immunohistochemically stained retinal wholemounts (*scale bar:* 250 μm). (**E**) Mean number of surviving RBPMS$^+$ RGC 3 days after purification and culture. *Asterisks* indicate significant difference at $P < 0.01$.

Retinal wholemounts were imaged using a Z1 Imager epifluorescent microscope and Axiocam HRc camera (Carl Zeiss, Inc., Thornwood, NY, USA) and RNA binding protein with multiple splicing (RBPMS)$^+$ cells were counted in three 0.33-mm^2 regions per retinal quadrant at 1, 2, and 3 mm from the optic nerve head (see Fig. 3C). An individual masked to the treatment group conducted counts manually. The mean number of RGC/image was derived from the 12 images, which made up 2.6% of the total retina (50 mm^2)[36] and was used to calculate RGC/mm^2 with each group consisting of 10 retinae from five different animals.

RNA Sequencing

RNAseq was performed by System Biosciences (#CSEQ400A-1) on sEV isolated from BMSC and fibroblasts (as detailed above), three replicates per group. sEV RNA was quantified by bioanalyzer small RNA assay (Agilent, Santa Clara, CA, USA) and libraries constructed and sequenced using Illumina NextSeq instrument with 1 × 75 bp single-end reads at an approximate depth of 10 to 15 million reads per sample. A scaling factor for a given sample was computed as the median of the ratio of its read count for each gene over its geometric mean across all samples. Raw read counts were divided by the factor associated with their samples for normalization. Unlike protein-coding genes/mRNA-seq data analysis in which only uniquely mapped reads are considered, the miRNA pipeline needs to allow multiple mapping of the same read to account for the multiple copies. Thus, normalization was done on the number of read alignments mapped to annotated gene features across samples instead of the number of mapped reads.

The RNAseq data was displayed as a heat map of the $\log_2$-fold change between fibroblast and BMSC sEV. A miRNA was considered differentially abundant when the $\log_2$-fold change was >2 or <−2. Using Ingenuity Pathway Analysis software, miRNA upregulated in BMSC sEV as well as their predicted targets were mapped. Predicted targets were only considered if they were experimentally observed findings and the mRNA/miRNA sequences were present in both rat and human.

Statistics

All statistical tests were performed using SPSS 17.0 (IBM SPSS, Inc., Chicago, IL, USA) and data presented as mean ± SEM with graphs constructed using Graphpad Prism 7.01 (Graphpad Prism, La Jolla, CA, USA). The Shapiro-Wilkes test was used to ensure all data were normally distributed before parametric testing using a 1-way ANOVA with a Tukey post hoc test. Statistical differences were considered significant at P values < 0.05.

Results

BMSC-Secreted sEV

sEV isolated from human BMSC and fibroblasts were visualized clearly by NanoSight and had a diameter of 100 to 120 nm, as expected for exosomes (Fig. 1B). Very few larger EV were detected and many of those that were detected were likely exosomal aggregates. While NanoSight cannot distinguish sEV from lipoprotein particles, Western blot data showed the absence of ApoA1 and ApoB, markers of lipoproteins, while markers of exosomes/sEV including Syntenin-1 and CD63 were detectable (Supplementary Fig. S2).

Intracameral Microbeads and Laser Photocoagulation of the Trabecular Meshwork Led to Elevations in IOP

Microbeads delivered ic (Group 2) led to a significant rise in IOP from 9.0 ± 0.5 mm Hg (Day 0) to 20.5 ± 2.4 mm Hg (Day 3), which remained high till the end of the experiment (14.2 ± 2.0 mm Hg; Day 56; Fig. 2A). In contrast, IOP in uninjected eyes (Group 1; 11.4 ± 0.7 mm Hg; Day 0) did not change significantly (10.3 ± 0.6 mm Hg; Day 56). The injection of sEV into the vitreous did not significantly ($P < 0.05$) affect the IOP in ic microbead-injected eyes.

Laser photocoagulation (Group 3) led to a significant rise in IOP from 9.0 ± 0.4 mm Hg (Day 0) to 25.0 ± 5.8 mm Hg (Day 7), which remained high until Day 17 (20.1 ± 4.2 mm Hg) but returned to baseline by the end of the experiment (11.1 ± 1.4 mm Hg; Day 21; Fig. 2B). In contrast, IOP in uninjected eyes (Group 1; 11.4 ± 0.7 mm Hg; Day 0) did not change significantly (11.7 ± 1.8 mm Hg; Day 21). The injection of sEV into the vitreous did not significantly ($P < 0.05$) affect the IOP in laser-photocoagulated eyes.

Intravitreal BMSC sEV Promote Neuroprotection

The intact cohort of Sprague Dawley had an RGC density of 2703.2 ± 73.3 RGC/mm^2, which was similar to values obtained in other studies.[37,38] The number of RBPMS$^+$ RGC at day 56 in retinal wholemounts decreased significantly in the ic microbead glaucoma model (1468.7 ± 186.3 RGC/mm^2) compared with intact eyes (2703.2 ± 73.3 RGC/mm^2; Fig. 3A). Monthly and weekly ivit injection of BMSC sEV provided significant neuroprotection of RGC (2113.8 ± 99.0 RGC/mm^2, 2438.4 ± 123.8 RGC/mm^2, respectively) but not single injection (1485.7 ± 27.3 RGC/mm^2). Monthly and weekly ivit injection of fibroblast sEV did not provide any neuroprotection to RGC (1485.0 ± 216.7 RGC/mm^2, 1563.4 ± 188.2 RGC/mm^2, respectively).

The number of RGC at day 21 in retinal wholemounts decreased significantly in the laser photocoagulation glaucoma model (1717.5 ± 173.6 RGC/mm^2) compared with intact eyes (2703.2 ± 73.3 RGC/mm^2; Fig. 3B). Single and weekly ivit injection of BMSC sEV provided significant neuroprotection of RGC (2416.3 ± 49.6 RGC/mm^2; 2609.3 ± 66.3 RGC/mm^2, respectively). This protective effect was partially abolished after ivit injection of sEV isolated from BMSC transfected with siAgo2 (2191.0 ± 23.8 μm) but was still present if sEV isolated from BMSC transfected with siScr were used (2550.2 ± 109.7 μm). Successful knockdown of AGO2 with siAgo2 was confirmed using Western blot (Supplementary Fig. S1). Single and weekly ivit injection of fibroblast sEV did not provide any neuroprotective effect to RGC (1975.6 ± 6 RGC/mm^2; 1850.6 ± 108.9 RGC/mm^2, respectively).

BMSC sEV Promote Neuroprotection of RGC Partially Through Direct Mechanisms

Purified RGC die very rapidly, due to the necessary axotomy when culturing along with the lack of present supporting cells. Untreated purified cultures of RGC showed significant death (25.7 ± 1.7 RGC/well) relative to the 5000 RGC plated after 3 days in culture (Fig. 3E). While fibroblast sEV provided little to no neuroprotective effect (60.7 ± 13.0 RGC/well) BMSC sEV elicited significant neuroprotection of (241 ± 17.7 RGC/well).

Intravitreal BMSC sEV Preserve RNFL Thickness/ RGC Axonal Density

The thickness of the RNFL at day 21 decreased significantly in the laser photocoagulation glaucoma model (31.8 ± 1.1 μm) compared with intact eyes (47.8 ± 1.8 μm; Fig. 4). Single and weekly ivit injection of BMSC sEV partially prevented degenerative thinning of the RNFL (46.0 ± 1.3 μm; 45.0 ± 1.8 μm, respectively). This protective effect was not present after ivit injection of sEV isolated from BMSC transfected with siAgo2 (32.4 ± 3.2 μm) but was still present if sEV isolated from BMSC transfected with siScr were used (46.8 ± 1.7 μm). Single and weekly ivit injection of fibroblast sEV did not prevent degenerative thinning of the RNFL (33.8 ± 1.5 μm; 34.0 ± 1.5 μm, respectively). There was no significant difference between baseline recordings of all groups as well as compared with intact at day 21 (data not shown).

Investigative Ophthalmology & Visual Science

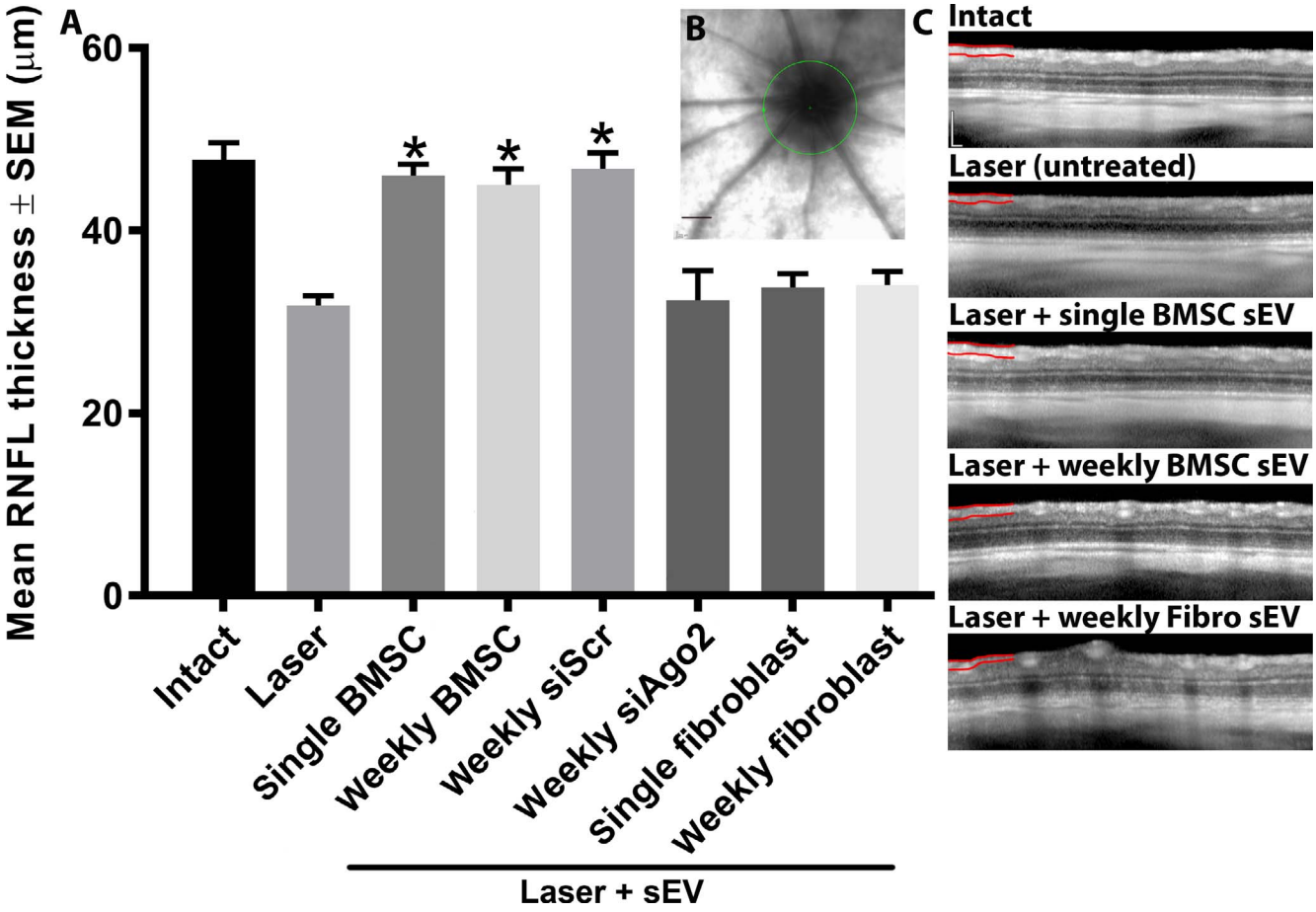

Figure 4. RNFL thickness measurements of rats. (**A**) Mean ± SEM RNFL thickness (μm) of rats measured by OCT in animals 21 days after laser photocoagulation. *Asterisks* indicate significant difference from injured/untreated at $P < 0.05$. (**B**) RNFL measurements were taken from around the optic nerve head (*green circle*; *scale bar*, 1 mm). (**C**) Representative OCT images of retina from which the RNFL (partially marked in *red*) measurements were taken (*scale bar:* 200 μm).

Intravitreal BMSC sEV Preserve pSTR Amplitude/ RGC Function

The amplitude of the pSTR at day 21 decreased significantly in the laser photocoagulation glaucoma model (23.6 ± 2.2 μv) compared with intact eyes (55.5 ± 0.7 μv; Fig. 5). Single and weekly ivit injection of BMSC sEV prevented degenerative loss of the pSTR (39.5 ± 5.1 μv; 44.3 ± 1.7 μv, respectively). This protective effect was not present after ivit injection of sEV isolated from BMSC transfected with siAgo2 (21.8 ± 1.4 μv) but was still present if sEV isolated from BMSC transfected with siScr were used (38.2 ± 2.1 μv). Single and weekly ivit injection of fibroblast sEV did not prevent degenerative loss of the pSTR (26.2 ± 1.1; 25.5 ± 2.5 μm, respectively). There was

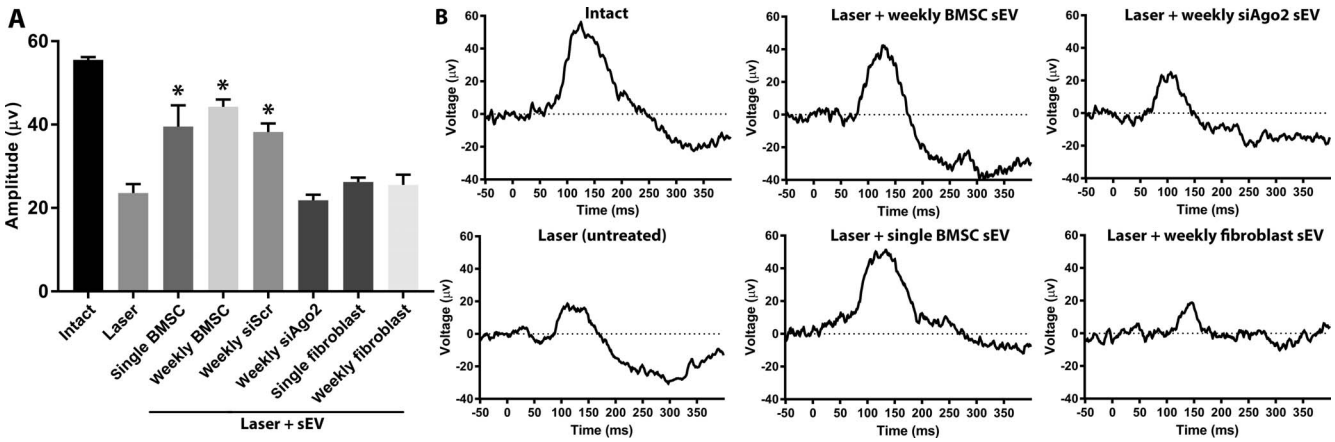

Figure 5. ERG measurements of pSTR. (**A**) Mean ± SEM amplitude (μv) of pSTR measured by ERG in animals 21 days after laser photocoagulation. *Asterisks* indicate significant difference from injured/untreated at $P < 0.05$. (**B**) Representative traces of pSTR.

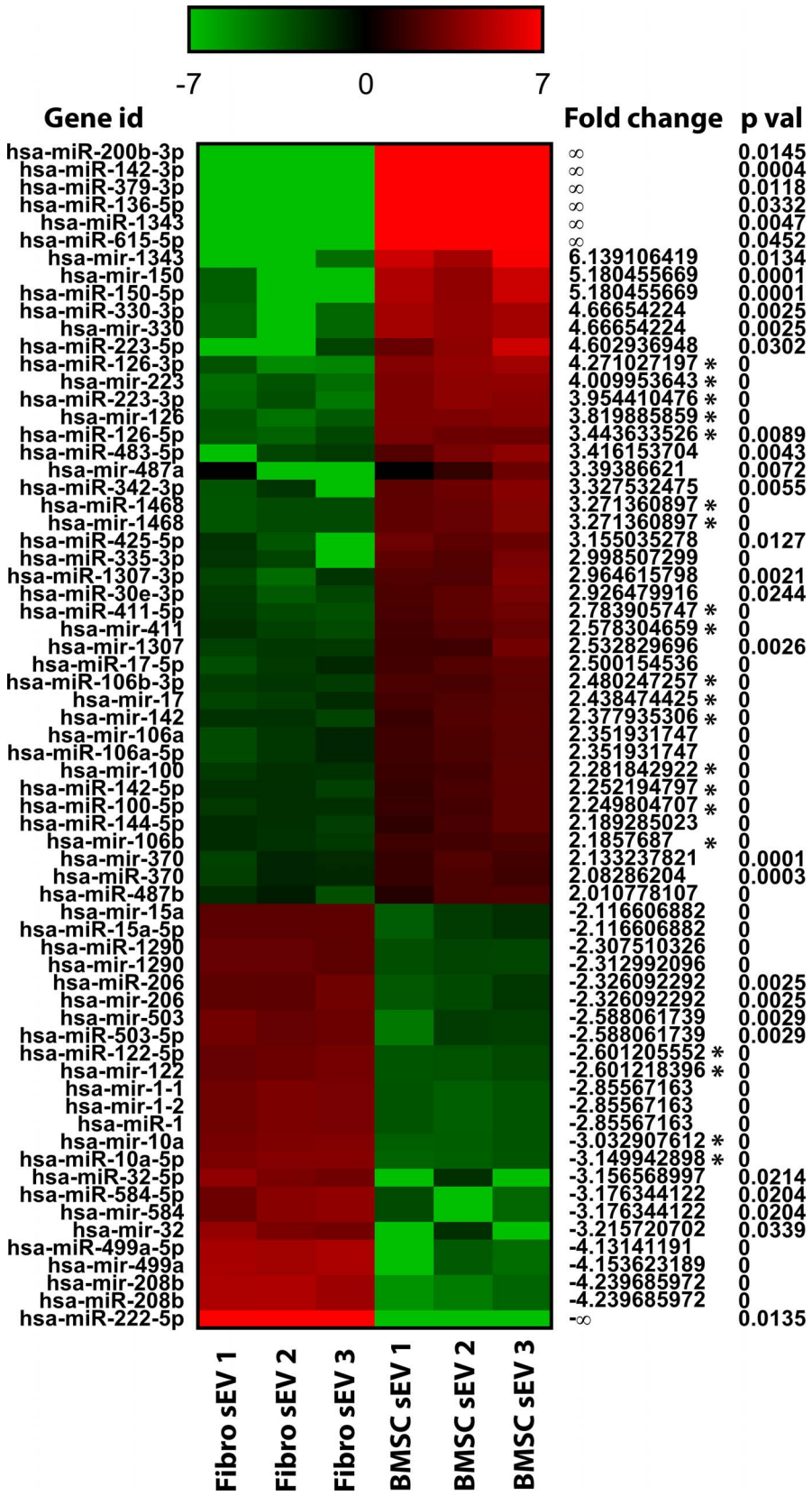

Figure 6. miRNA abundance heat map profile. A comparison of the miRNA abundance profile in BMSC sEV and fibroblast sEV, displayed as a heat map of the $\log_2$-fold change. *Red* indicates high comparative abundance, whereas *green* denotes low comparative abundance. Average $\log_2$-fold change, an abundance value >200 reads per million (*Asterisk*) as well as *P* value are given. miRNA with >2 or <−2 fold change only are shown.

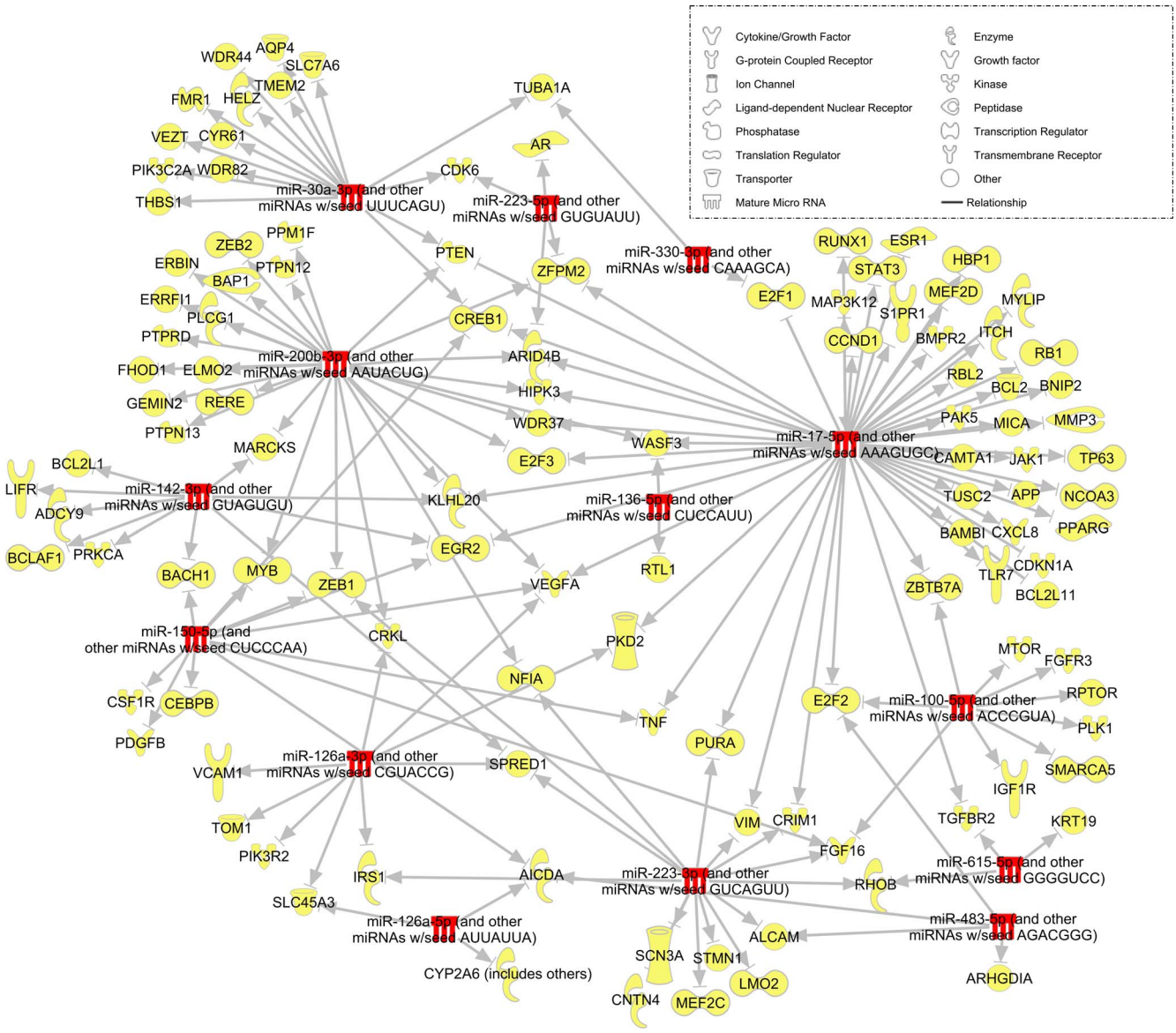

Figure 7. miRNA targeting network. Schematic diagram displaying miRNA (*red*) upregulated in BMSC sEV and their experimentally observed mRNA targets (*yellow*). Targeted genes were identified with ingenuity pathway analysis software and filtered for experimentally observed interactions and, miRNA/mRNA sequences identified in both human and rat.

Table 2. Enriched Signaling Pathways Regulated by miRNA Abundant in sEV

Term	No. of Genes A/B	*P* Value
IL-15 signaling	11/76	<0.001
JAK/STAT pathway	10/83	<0.001
HGF signaling	11/115	<0.001
PTEN signaling	11/119	<0.001
IL-8 signaling	13/197	<0.001
FGF signaling	10/90	<0.001
PDGF signaling	10/90	<0.001
EGF signaling	9/68	<0.001

Experimentally observed (1) and predicted (2) mRNA targets of miRNA overabundant in BMSC sEV compared with fibroblast sEV, displayed as the most enriched signaling pathways.

no significant difference between baseline recordings of all groups as well as compared with intact at day 21 (data not shown).

RNAseq Data

RNAseq detected 43 miRNA that were overabundant in BMSC sEV by >2 (log_2-fold change) compared with fibroblast sEV and 24 miRNA that were overabundant in fibroblast sEV by >2 compared with BMSC sEV (Fig. 6). Using ingenuity pathway analysis, targets of the abundant miRNA were predicted (Fig. 7) and the most enriched/targeted-signaling pathway identified (Table 2).

Discussion

The present study demonstrates that sEV derived from BMSC promote significant neuroprotection of $RBPMS^+$ RGC in two

separate and distinct models of glaucoma while protecting against RNFL degeneration and pSTR loss. We attributed the protective effect at least partially to the miRNA found within sEV, a finding corroborated by our previous study in an ONC rat model.[22] We used two models of glaucoma in this study to minimize the limitations that are present in every glaucoma model. For example, the laser model suffers from being a short, recoverable rise in IOP, whereas the ic microbead model, while being characterized by a persistent rise in IOP, suffers from opacities due to the beads in the anterior chamber, rendering ERG and OCT unreliable. As not every animal responded with elevated ocular hypertension, additional animals were run to ensure each treatment subgroup consisted of five animals/10 eyes.

While MSC are currently undergoing clinical trials to test their efficacy is various ocular diseases,[13] their sEV have been demonstrated safe in a recent clinical trial.[39] Systemic delivery of UCB-MSC–derived sEV into patients with chronic kidney disease proved not only safe but also, significantly improved kidney function while reducing inflammation.

Our previous study showed that sEV integrate into cells within the ganglion cell layer, leading us to speculate that the effect was direct, independent of non-RGC retinal cell mediators. Our current findings demonstrate that in a purified culture, RGC undergo the stereotypical 95% death after 4 days[40,41] while treatment with sEV from BMSC, but not fibroblasts, promoted significant RGC neuroprotection. This further confirms that at least part of the neuroprotective effect is mediated through direct sEV-RGC interactions. It should be noted that the RGC are purified based on their expression of Thy-1, a marker expressed in only 80% of RGC yet expressed in cholinergic amacrine cells.[42] While 5000 RGC are plated, only approximately 30% attach to the plate.[40] Thus, one criticism of the purified RGC culture is it likely does not encompass every RGC subtype.

The present study corroborates our previous findings that showed BMSC sEV–mediated protection of RGC after ONC in the rat. While a recent review highlights the growing trend in ocular exosome/sEV research,[43] few studies exist testing sEV as a treatment in the eye. In a mouse retinopathy model characterized by degeneration of vasculature and cessation of their development, ivit delivery of exosomes derived from endothelial colony-forming cells promoted significant angiogenesis and reductions in avascular areas.[44] Interestingly, authors identified significant modulation of gene expression in endogenous endothelial cells and related this effect to the miRNA present in the exosomes. In a mouse model of experimental autoimmune uveitis, systemic administration of BMSC exosomes promoted significant reduction in inflammation.[27] ivit injection of UCB-MSC or ADSC exosomes into a mouse model of retinal laser injury promoted significant neuroprotection while suppressing an inflammatory response and improving visual function.[30] Application of exosomes derived from mouse fibroblast L cells shortly after optic nerve injury promoted robust axonal regeneration, which was strongly reduced in Wnt10b-deleted animals.[45]

It is still unclear how long exosomes/sEV remain after administration into biological tissues, such as the vitreous. We previously demonstrated therapeutic efficacy from weekly ivit injections,[22] whereas a separate study used a single intravenous administration[27] at a much higher dose (15×10^9 exosomes), demonstrating a therapeutic effect 21 days later in an experimentally autoimmune uveitis model.

Ideally, ocular treatment should be long lasting to minimize repeat injections and while there is a precedent for cell therapy to have long lasting effects, no studies have assessed the longevity of transplanted sEV. We used several different treatment schedules in attempt to address this question, injecting once, weekly, and monthly. As we previously demonstrated,[22] weekly ivit injections proved effective in all measured endpoints. Interestingly, injections separated by 1 month also proved equally effective although a nonsignificant trend toward a reduced neuroprotective effect compared with weekly injections was observed in the microbead model. Because the microbead model takes place over 56 days, we also tested a single injection. The neuroprotective effects of BMSC sEV were completely absent without a second injection after 1 month, suggesting that BMSC sEV activity drops dramatically after approximately 1 month in the vitreous. This timeframe likely represents both the duration sEV reside in the vitreous and the length of time the miRNA-mediated gene regulation lasts.

AGO2 knockdown–mediated depletion of miRNA partially inhibited the positive effects elicited by sEV evident by the reduced RGC numbers, RNFL thickness, and pSTR amplitude; with this suggestion that miRNA are integral to the mechanism, we performed miRNAseq on BMSC sEV to aid in the potential identification of candidates. We were able to identify candidate miRNA that were more abundant in BMSC sEV in comparison to fibroblast sEV. Several recent studies have analyzed the miRNA content of MSC sEV. The first study identified 11 miRNA present in UCB-MSC–derived sEV via microarray[46] while the second study detailed the top 100 most abundant miRNA using RNAseq,[47] demonstrating much overlap. These miRNA were also detected by our RNAseq, however only *MIR-100-5P* and *MIR-106A-5P* were significantly more abundant in BMSC sEV in comparison to fibroblast sEV. A third study performed RNAseq on human ADSC–derived sEV to identify the miRNA potentially responsible for the observed anticancer properties.[48] Several of the miRNA that were detected were also identified in the present study including *MIR-1246* and *MIR-269-5P* however, these miRNA were also found in equal or greater abundance within fibroblast sEV, suggesting that they may not be integral to the neuroprotective effects elicited. One miRNA detected was also present in our data, *MIR-486-5P*, and was more abundant (1.8-$\log_2$ fold change higher) in BMSC sEV compared with fibroblast sEV, as well as being one of the most abundant miRNA. This result has been further confirmed by a separate RNAseq analysis performed on both human BMSC and ADSC[23] as well as demonstrating that abundant miRNA differed between each MSC source.

While abundance of particular BMSC-miRNA in comparison to fibroblasts is critical for the identification of candidates, sEV-mediated delivery of miRNA to the retina can only be effective if the packaged miRNA are not already abundantly present in the injured retina. For example, one recent study analyzed rat retina 7 days after ocular hypertension,[49] using microarray to detect overabundant miRNA, whereas a separate study analyzed 16 human retina from cadavers without any retinal pathology, determining the 40 most highly abundant.[50] From these studies and the identified miRNA of the present study; *MIR-144-5P*, *MIR-126-5P*, and *MIR-100-5P* were found to also be overabundant in BMSC sEV. Because these miRNA are already present in the retina, their contribution following sEV-mediated delivery is likely minimal. In contrast, it has been demonstrated that in the glaucomatous rat retina, several miRNA are downregulated including *mir-106b*,[51] which we found to be abundant in BMSC sEV. It is feasible that downregulation of miRNA has some role in the pathology of glaucoma and delivery of these miRNA via BMSC sEV prevents RGC degeneration. One caveat to the above studies is that miRNA abundance was quantified in total retina as opposed to purified RGC. Currently, no such study exists that provides a detailed analysis of the miRNA present in RGC both before, and after injury.

While we believe that miRNA play an integral role in the sEV-mediated neuroprotection of RGC, it is important to note that miRNA have been found associated with other molecules including protein aggregates[52] and virus particles,[53] both of which could be found within sEV preparation. Because the miRNA associated with these protein aggregates[52] also contains AGO2, it is possible that the diminished therapeutic benefit after AGO2 knockdown is due to these miRNA as well as sEV associated miRNA. Furthermore, after knockdown of AGO2 (siAgo2), sEV still trended toward neuroprotection. As siAgo2 yielded an incomplete (>70%) AGO2 knockdown, it is possible that residual miRNA function was present and responsible for this trend in RGC neuroprotection. Alternatively, non-miRNA components of the BMSC sEV cargo may indeed contribute some beneficial effects and include not only mRNA but approximately 5000 proteins.[24] Recently, BMSC-derived sEV were shown to express an isoform of PDGF, referred to as PDGF-D.[54] Because PDGF was been shown to be secreted from BMSC and promote significant RGC neuroprotection,[14] it is possible that the PDGF loaded in sEV elicits similar effects.

In conclusion, BMSC sEV promote neuroprotection and functional preservation of RGC in two rat glaucomatous models. While ivit injection of sEV did not directly affect IOP, their neuroprotective efficacy makes them a good candidate as an adjunctive therapy to IOP-lowering medications, and thus, a potential future treatment for glaucoma.

Acknowledgments

The authors thank Robert Fariss, PhD, for his assistance with laser model, Haohua Qian, PhD, for his assistance with the ERG and OCT, Jennifer Jones, PhD, for her assistance with the NanoSight, Heather Mak, PhD, and Christopher Leung, PhD, for their help with RGC isolation protocol, and Sammy Bennet for his assistance in immunohistochemistry and cell counting.

Supported by the Intramural Research Programs of the National Eye Institute (Bethesda, MD, USA).

Disclosure: **B. Mead**, None; **J. Amaral**, None; **S. Tomarev**, None

References

1. Tham Y-C, Li X, Wong TY, Quigley HA, Aung T, Cheng C-Y. Global prevalence of glaucoma and projections of glaucoma burden through 2040. *Ophthalmology*. 2014;121:2081–2090.
2. Friedenstein AJ, Chailakhjan RK, Lalykina KS. The development of fibroblast colonies in monolayer cultures of guinea-pig bone marrow and spleen cells. *Cell Tissue Kinet*. 1970;3:393–403.
3. Zuk PA, Zhu M, Mizuno H, et al. Multilineage cells from human adipose tissue: implications for cell-based therapies. *Tissue Eng*. 2001;7:211–228.
4. Erices A, Conget P, Minguell JJ. Mesenchymal progenitor cells in human umbilical cord blood. *BrJ Haematol*. 2000;109:235–242.
5. Gronthos S, Mankani M, Brahim J, Robey PG, Shi S. Postnatal human dental pulp stem cells (DPSCs) in vitro and in vivo. *Proc Natl Acad Sci U S A*. 2000;97:13625–13630.
6. Mead B, Logan A, Berry M, Leadbeater W, Scheven BA. Intravitreally transplanted dental pulp stem cells promote neuroprotection and axon regeneration of retinal ganglion cells after optic nerve injury. *Invest Ophthalmol Vis Sci*. 2013;54:7544–7556.
7. Mead B, Logan A, Berry M, Leadbeater W, Scheven BA. Paracrine-mediated neuroprotection and neuritogenesis of axotomised retinal ganglion cells by human dental pulp stem cells: comparison with human bone marrow and adipose-derived mesenchymal stem cells. *PLoS One*. 2014;9:e109305.
8. Mead B, Hill LJ, Blanch RJ, et al. Mesenchymal stromal cell-mediated neuroprotection and functional preservation of retinal ganglion cells in a rodent model of glaucoma. *Cytotherapy*. 2016;18:487–496.
9. Johnson TV, Bull ND, Hunt DP, Marina N, Tomarev SI, Martin KR. Neuroprotective effects of intravitreal mesenchymal stem cell transplantation in experimental glaucoma. *Invest Ophthalmol Vis Sci*. 2010;51:2051–2059.
10. Mesentier-Louro LA, Zaverucha-do-Valle C, da Silva-Junior AJ, et al. Distribution of mesenchymal stem cells and effects on neuronal survival and axon regeneration after optic nerve crush and cell therapy. *PLoS One*. 2014;9:e110722.
11. Emre E, Yuksel N, Duruksu G, et al. Neuroprotective effects of intravitreally transplanted adipose tissue and bone marrow-derived mesenchymal stem cells in an experimental ocular hypertension model. *Cytotherapy*. 2015;17:543–549.
12. Tan HB, Kang X, Lu SH, Liu L. The therapeutic effects of bone marrow mesenchymal stem cells after optic nerve damage in the adult rat. *Clin Interv Aging*. 2015;10:487–490.
13. Mead B, Berry M, Logan A, Scott RAH, Leadbeater W, Scheven BA. Stem cell treatment of degenerative eye disease. *Stem Cell Res*. 2015;14:243–257.
14. Johnson TV, Dekorver NW, Levasseur VA, et al. Identification of retinal ganglion cell neuroprotection conferred by platelet-derived growth factor through analysis of the mesenchymal stem cell secretome. *Brain*. 2014;137(pt 2):503–519.
15. Colombo M, Raposo G, Thery C. Biogenesis, secretion, and intercellular interactions of exosomes and other extracellular vesicles. *Annu Rev Cell Dev Biol*. 2014;30:255–289.
16. Thery C, Amigorena S, Raposo G, Clayton A. Isolation and characterization of exosomes from cell culture supernatants and biological fluids. *Curr Protoc Cell Biol*. 2006; Chapter 3: Unit 3.22.
17. Kowal J, Arras G, Colombo M, et al. Proteomic comparison defines novel markers to characterize heterogeneous populations of extracellular vesicle subtypes. *Proc Natl Acad Sci U S A*. 2016;113:E968–E977.
18. Valadi H, Ekstrom K, Bossios A, Sjostrand M, Lee JJ, Lotvall JO. Exosome-mediated transfer of mRNAs and microRNAs is a novel mechanism of genetic exchange between cells. *Nat Cell Biol*. 2007;9:654–672.
19. Gregory RI, Chendrimada TP, Cooch N, Shiekhattar R. Human RISC couples microRNA biogenesis and posttranscriptional gene silencing. *Cell*. 2005;123:631–640.
20. Lv Z, Wei Y, Wang D, Zhang C-Y, Zen K, Li L. Argonaute 2 in Cell-secreted microvesicles guides the function of secreted mirnas in recipient cells. *PLoS One*. 2014;9:e103599.
21. Zhang Y, Chopp M, Liu XS, et al. Exosomes derived from mesenchymal stromal cells promote axonal growth of cortical neurons. *Mol Neurobiol*. 2017;54:2659–2673.
22. Mead B, Tomarev S. Bone marrow-derived mesenchymal stem cells-derived exosomes promote survival of retinal ganglion cells through miRNA-dependent mechanisms. *Stem Cells Transl Med*. 2017;6:1273–1285.
23. Baglio SR, Rooijers K, Koppers-Lalic D, et al. Human bone marrow- and adipose-mesenchymal stem cells secrete exosomes enriched in distinctive miRNA and tRNA species. *Stem Cell Res Ther*. 2015;6:127.
24. Eirin A, Zhu X-Y, Puranik AS, et al. Comparative proteomic analysis of extracellular vesicles isolated from porcine adipose tissue-derived mesenchymal stem/stromal cells. *Sci Rep*. 2016;6:36120.
25. Anderson JD, Johansson HJ, Graham CS, et al. comprehensive proteomic analysis of mesenchymal stem cell exosomes reveals modulation of angiogenesis via nuclear factor-kappaB signaling. *Stem Cells*. 2016;34:601–613.

26. Eirin A, Riester SM, Zhu XY, et al. MicroRNA and mRNA cargo of extracellular vesicles from porcine adipose tissue-derived mesenchymal stem cells. *Gene*. 2014;551:55–64.
27. Shigemoto-Kuroda T, Oh JY, D-k, Kim et al. MSC-derived extracellular vesicles attenuate immune responses in two autoimmune murine models: type 1 diabetes and uveoretinitis. *Stem Cell Rep*. 2017;8:1214–1225.
28. Bai L, Shao H, Wang H, et al. Effects of mesenchymal stem cell-derived exosomes on experimental autoimmune uveitis. *Sci Rep*. 2017;7:4323.
29. Nagaishi K, Mizue Y, Chikenji T, et al. Mesenchymal stem cell therapy ameliorates diabetic nephropathy via the paracrine effect of renal trophic factors including exosomes. *Sci Rep*. 2016;6:34842.
30. Yu B, Shao H, Su C, et al. Exosomes derived from MSCs ameliorate retinal laser injury partially by inhibition of MCP-1. *Sci Rep*. 2016;6:34562.
31. Lai RC, Arslan F, Lee MM, et al. Exosome secreted by MSC reduces myocardial ischemia/reperfusion injury. *Stem Cell Res*. 2010;4:214–222.
32. Wang N, Chen C, Yang D, et al. Mesenchymal stem cells-derived extracellular vesicles, via miR-210, improve infarcted cardiac function by promotion of angiogenesis. *Biochim Biophys Acta*. 2017;1863:2085–2092.
33. Borges F, Schor N, Novaes A. Mesenchymal stem cell exosomes transfer microRNA and protect injured tubular epithelial cells (E-Abstract 670.8). *FASEB J*. 2015;29.
34. Smedowski A, Pietrucha-Dutczak M, Kaarniranta K, Lewin-Kowalik J. A rat experimental model of glaucoma incorporating rapid-onset elevation of intraocular pressure. *Sci Rep*. 2014;4:5910.
35. Levkovitch-Verbin H, Quigley HA, Martin KR, Valenta D, Baumrind LA, Pease ME. Translimbal laser photocoagulation to the trabecular meshwork as a model of glaucoma in rats. *Invest Ophthalmol Vis Sci*. 2002;43:402–410.
36. Salinas-Navarro M, Mayor-Torroglosa S, Jimenez-Lopez M, et al. A computerized analysis of the entire retinal ganglion cell population and its spatial distribution in adult rats. *Vision Res*. 2009;49:115–126.
37. Rodriguez AR, Muller LPD, Brecha NC. The RNA binding protein RBPMS is a selective marker of ganglion cells in the mammalian retina. *J Comp Neurol*. 2014;522:1411–1443.
38. Kwong JM, Quan A, Kyung H, Piri N, Caprioli J. Quantitative analysis of retinal ganglion cell survival with RBPMS immunolabeling in animal models of optic neuropathies. *Invest Ophthalmol Vis Sci*. 2011;52:9694–9702.
39. Nassar W, El-Ansary M, Sabry D, et al. Umbilical cord mesenchymal stem cells derived extracellular vesicles can safely ameliorate the progression of chronic kidney diseases. *Biomater Res*. 2016;20:21.
40. Xu Z, Cho H, Hartsock M, et al. Neuroprotective role of Nrf2 for retinal ganglion cells in ischemia-reperfusion. *J Neurochem*. 2015;133:233–241.
41. Welsbie DS, Yang Z, Ge Y, et al. Functional genomic screening identifies dual leucine zipper kinase as a key mediator of retinal ganglion cell death. *Proc Natl Acad Sci U S A*. 2013;110:4045–4050.
42. Mead B, Tomarev S. Evaluating retinal ganglion cell loss and dysfunction. *Exp Eye Res*. 2016;151:96–106.
43. Klingeborn M, Dismuke WM, Bowes Rickman C, Stamer WD. Roles of exosomes in the normal and diseased eye. *Prog Retin Eye Res*. 2017;59:158–177.
44. Dellett M, Brown ED, Guduric-Fuchs J, et al. MicroRNA-containing extracellular vesicles released from endothelial colony-forming cells modulate angiogenesis during ischaemic retinopathy. *J Cell Mol Med*. 2017;21:3405–3419.
45. Tassew NG, Charish J, Shabanzadeh AP, et al. Exosomes mediate mobilization of autocrine Wnt10b to promote axonal regeneration in the injured CNS. *Cell Rep*. 2017;20:99–111.
46. Sun L, Li D, Song K, et al. Exosomes derived from human umbilical cord mesenchymal stem cells protect against cisplatin-induced ovarian granulosa cell stress and apoptosis in vitro. *Sci Rep*. 2017;7:2552.
47. Qian X, Xu C, Fang S, et al. Exosomal microRNAs derived from umbilical mesenchymal stem cells inhibit hepatitis C virus infection. *Stem Cells Transl Med*. 2016;5:1190–1203.
48. Reza AMMT, Choi Y-J, Yasuda H, Kim J-H. Human adipose mesenchymal stem cell-derived exosomal-miRNAs are critical factors for inducing anti-proliferation signalling to A2780 and SKOV-3 ovarian cancer cells. *Sci Rep*. 2016;6:38498.
49. Wang J, Valiente-Soriano FJ, Nadal-Nicolás FM, et al. MicroRNA regulation in an animal model of acute ocular hypertension. *Acta Ophthalmol*. 2017;95:e10–e21.
50. Karali M, Persico M, Mutarelli M, et al. High-resolution analysis of the human retina miRNome reveals isomiR variations and novel microRNAs. *Nucleic Acids Res*. 2016;44:1525–1540.
51. Jayaram H, Cepurna WO, Johnson EC, Morrison JC. MicroRNA expression in the glaucomatous retina. *Invest Ophthalmol Vis Sci*. 2015;56:7971–7982.
52. Arroyo JD, Chevillet JR, Kroh EM, et al. Argonaute2 complexes carry a population of circulating microRNAs independent of vesicles in human plasma. *Proc Natl Acad Sci U S A*. 2011;108:5003–5008.
53. Bogerd HP, Kennedy EM, Whisnant AW, Cullen BR. Induced packaging of cellular microRNAs into HIV-1 virions can inhibit infectivity. *Mbio* 2017;8:pii:e02125-16.
54. Huang F, Yao YL, Wu JH, et al. Effect of mesenchymal stem cell derived exosomes carrying PDGFD on lung cancer. *Int J Clin Exp Pathol*. 2017;10:224–232.

Investigative Ophthalmology & Visual Science